Anomalous fast ion losses at high β on the tokamak fusion test reactor

E. D. Fredrickson, M. G. Bell, R. V. Budny, D. S. Darrow, and R. White

Citation: Physics of Plasmas **22**, 032501 (2015); doi: 10.1063/1.4907656
View online: http://dx.doi.org/10.1063/1.4907656
View Table of Contents: http://scitation.aip.org/content/aip/journal/pop/22/3?ver=pdfcov
Published by the AIP Publishing

Anomalous fast ion losses at high β on the tokamak fusion test reactor

E. D. Fredrickson, M. G. Bell, R. V. Budny, D. S. Darrow, and R. White
Princeton Plasma Physics Laboratory, Princeton, New Jersey 08543, USA

(Received 18 November 2014; accepted 21 January 2015; published online 2 March 2015)

This paper describes experiments carried out on the Tokamak Fusion Test Reactor (TFTR) [R. J. Hawryluk *et al.*, Plasma Phys. Controlled Fusion 33, 1509 (1991)] to investigate the dependence of β-limiting disruption characteristics on toroidal field strength. The hard disruptions found at the β-limit in high field plasmas were not found at low field, even for β's 50% higher than the empirical β-limit of $\beta_n \approx 2$ at high field. Comparisons of experimentally measured β's to TRANSP simulations suggest anomalous loss of up to half of the beam fast ions in the highest β, low field shots. The anomalous transport responsible for the fast ion losses may at the same time broaden the pressure profile. Toroidal Alfvén eigenmodes, fishbone instabilities, and Geodesic Acoustic Modes are investigated as possible causes of the enhanced losses. Here, we present the first observations of high frequency fishbones [F. Zonca *et al.*, Nucl. Fusion **49**, 085009 (2009)] on TFTR. The interpretation of Axi-symmetric Beam-driven Modes as Geodesic Acoustic Modes and their possible correlation with transport barrier formation are also presented. © *2015 AIP Publishing LLC*.
[http://dx.doi.org/10.1063/1.4907656]

I. INTRODUCTION

The Tokamak Fusion Test Reactor (TFTR)[1] routinely operated near the ideal β-limit, and while feed-forward programming was effective in avoiding most disruptions, the approach was not 100% effective. Disruptions released deuterium from sub-surface layers of plasma facing components (PFCs), which was then absorbed on the surface of the graphite limiter tiles. The surface condition of the inboard graphite divertor on TFTR was strongly correlated with energy confinement and plasma performance. Multiple low density helium shots were required to recondition the limiter following disruptions. To minimize the impact of disruption experiments on limiter conditions, experiments to study the physics of β-limits were done at low field (2 T) where the energies released in the disruptions were much lower than at full field. It was discovered that the beta limit was significantly higher at lower field (Fig. 1), and that the maximum beta was limited by loss of energy confinement rather than hard disruptions. The high field (5 T) shot in Fig. 1 (red curves) was terminated by a thermal quench, triggering a current quench.[2–5] The beta limit at low field resulted from a "soft" confinement collapse and no current quench (black curves).

Since, ultimately, the global beta limit is imposed by local violations of MHD stability, experimental determination of the pressure profile shape is important for understanding ideal stability near the beta limit. In these beam-heated plasmas, a large fraction (up to 45%) of the stored energy is in the super-thermal beam ion population. At high field, in the absence of fishbones[6] or kink/tearing modes,[7,8] classical processes (as incorporated in the TRANSP[9] and NUBEAM[10] codes) seem adequate to describe fast ion confinement. However, in these low field and high β plasmas, TRANSP predicts larger than measured betas and neutron rates, an observation which suggests additional, anomalous, fast ion loss. The fast ion transport processes responsible for the losses will also likely redistribute the confined fast ions, reducing the pressure peakedness and thus increasing the beta limits. This observation made stability analysis difficult, as it could no longer be assumed that the fast ion distribution, a substantial contribution to total plasma pressure, could be calculated with a purely classical model for the thermalization of beam-injected ions. A second complication was that in both the high and low field plasmas, MSE pitch-angle measurements found that q(0) was significantly less than unity, typical for TFTR supershots.[11] This is consistent with other evidence such as evolution of the sawtooth inversion radii and TRANSP current evolution simulations. The $q(0) < 1$ makes even moderate β plasmas unstable to the ideal internal kink. Nevertheless, these plasmas made at low field reached $\beta_n > 3$ or $\beta_n/4l_i > 0.6$.

There are several potential explanations for this experimentally observed toroidal field dependence of ®-limits on toroidal field. At high toroidal field, the initial thermal

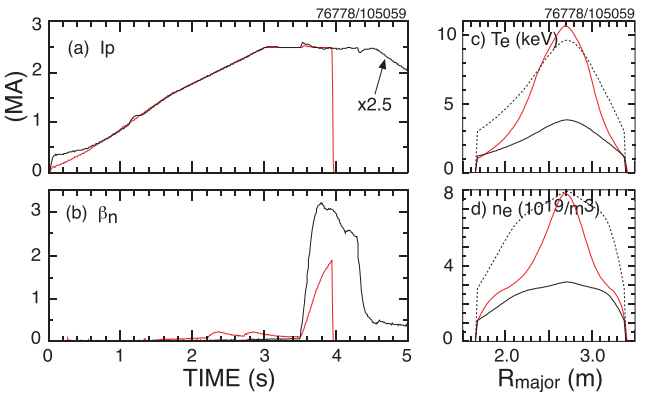

FIG. 1. Waveforms comparing high beta shots at 5 T (red curves) and 2 T (black curves) with same q(a). Dashed profiles show electron temperature and density scaled by 2.5.

quench is triggered by ballooning modes localized toroidally by an internal kink-ballooning mode.[3,4] At lower field, finite Larmor radius effects may stabilize the intermediate-n ballooning modes responsible for triggering the disruptions at high field. Or, an alternative explanation is that the lower stored energy at the ®-limit in the low field shots means the interaction of the plasma with plasma-facing components is less severe than at high field, which may be responsible for soft vs. hard ®-limits. This may be a concern for ITER which is expected to have more than 20 times the stored plasma energy, but less than four times the PFC surface area of, for example, JET.

At low and high field, classical fast ion confinement is seen for $\beta_n < 2$, while anomalous fast ion losses are seen in plasmas with $\beta_n > 2$ ($\beta_{pol} > 0.9$). The losses are inferred from comparisons of TRANSP predictions of the thermal and fast ion β's compared to experimental measurements of total beta. The TRANSP calculation of β assumes classical fast-ion confinement plus the measured electron beta and ion beta inferred from electron and ion temperature measurements and measurements of the electron density and Z_{eff} profile (from which the ratio of electron to ion density is inferred).

The onset of the stored energy discrepancy above $\beta_{pol} \approx 0.9$ is illustrated in Figure 2 where the peak poloidal betas (diamagnetic and equilibrium) from experimental measurements are compared to the TRANSP predictions (without anomalous fast ion diffusion) for a wide range of high and low field shots. For the plasma conditions described here, TRANSP very accurately predicts total betas for plasmas with $\beta_n < 2$, but increasingly overestimates β_{pol} and neutron rates for β_n's larger than this. In Fig. 2, the β_{pol} appears to saturate just below the limit predicted by Troyon, $\beta_{pmax} = 0.14\ R_p\ q_s/a_p \approx 1.7$, for large aspect ratio, circular cross-section plasmas.[12]

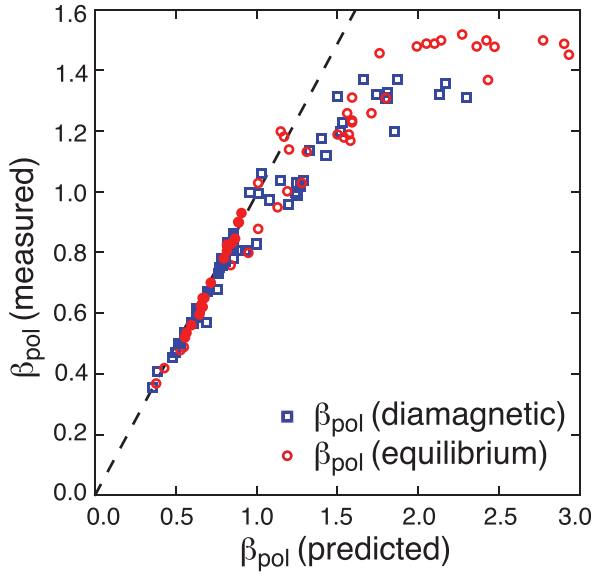

FIG. 2. Comparison of measured to predicted β_{pol} at time of peak energy for beam-heating power scans for two plasma conditions (1MA, 2 T, open symbols) and (2.5 MA, 5 T, solid symbols).

This paper will focus on the inferred fast ion loss and examine a variety of fast-ion-driven instabilities which might be responsible for the losses. Ideal MHD stability analysis of the discharges will not be presented, due to uncertainties in the fast ion pressure profile; a significant portion of the total pressure. We begin with a general description of the experimental conditions and compare TRANSP simulations to the experimental evolution of stored energy, anisotropy and, where applicable, neutron rates in Sec. II. We introduce *ad hoc* models for anomalous fast ion redistribution to match the experimental β_{pol}, anisotropy and neutron rate evolutions. In Sec. III, the various forms of energetic particle driven instabilities seen in these plasmas are described, and the correlation with inferred anomalous losses is discussed. Section IV summarizes and discusses the data and analysis presented here.

II. β-LIMIT SCALING WITH TOROIDAL FIELD STRENGTH

The highest performance plasmas on TFTR were limited by available neutral beam power, energy confinement and stability. That is, in the highest confinement conditions reached on TFTR, there was just enough neutral beam heating power to reach the beta limit (e.g., Fig. 1) at the highest currents and fields. The best confinement regimes on TFTR had very peaked pressure and current profiles with $q(0) < 1$. The beta limiting disruption was triggered by a moderate n ballooning mode toroidally localized by the presence of an $n = 1$ internal kink. The ballooning modes caused a partial thermal quench, typically releasing about 20% of the plasma stored energy. The impact of this $\approx$1 MJ of energy on the PFCs led to a release of cold gas and impurities from the limiter and walls, causing a thermal collapse of the plasma, leading to a fast current quench.[5] The difficulty in reaching the beta limit at full parameters, together with the necessity for reconditioning the limiter after major disruptions, encouraged the study of beta limit disruptions at reduced parameters.

For consistency in comparison of the high and low field disruptions, the low field target plasma current and field were scaled from the standard high performance configuration of 2.5 MA of plasma current, a toroidal field of 5 T and a major radius of 2.52 m, minor radius of 0.87 m ($A \approx 2.9$). The scaled plasma current was chosen to be 1 MA to give reasonable beam-ion confinement, so that the scaled toroidal field is 2 T (with the same plasma dimensions). The ECE instruments[13,14] for measurement of the electron temperature work reasonably well at 2 T, although not as well as at 5 T. The Charge-Exchange Recombination Spectroscopy (CHERS) diagnostic[15] for ion temperature, plasma rotation, and carbon impurity density profile measurements, and the Multi-channel Infra-Red Interferometer (MIRI) diagnostic[16] for electron density profile are unaffected by the lower field.

Two of these low field shots will be described in detail for comparison to the high field disruptions. The first case has similar beta to the high field disruption, but remains stable. The second has higher beam power and reaches much higher β, followed by a "soft" β or energy confinement collapse. The TRANSP simulations of the beta evolutions are

compared in Figs. 3–5. Shown in Fig. 3 is the TRANSP modeling (red) for a high field, β-limit disruption. Figure 4 shows a low field shot reaching a similar β, without collapse or disruption and in Fig. 5 is a low field shot with roughly 50% higher beta which suffers from a soft beta collapse or "confinement saturation".

The TRANSP analysis of high performance, high field discharges typically finds reasonably good agreement, in absence of MHD instabilities, between the measured stored energy, pressure anisotropy and measured D-T and D-D neutron rates.[9] This is illustrated in Fig. 3 where the time evolution of these parameters as calculated in TRANSP are compared to the measured values. The 14 MeV neutron rate in Fig. 3(b) results from nearly equal D and T neutral beam injection. The calculated DT reaction rate is not sensitive to the trace amount of thermal T from wall recycling in the plasma. In Fig. 3(c) the diamagnetic β_{pol}, i.e., from the perpendicular energy, is compared to the TRANSP calculation and in Fig. 3(d) a similar comparison is made of the equilibrium β_{pol}. The equilibrium β_{pol} is a weighted average of the perpendicular and parallel pressures, favoring the parallel pressure. Thus, the difference between the diamagnetic and equilibrium β_{pol}'s is a measure of the plasma anisotropy. The neutral beam heating sources on TFTR are oriented for co-tangential and counter-tangential injection, resulting in a fast ion distribution weighted in the parallel direction. This is reflected in the equilibrium β_{pol} being greater than the diamagnetic β_{pol}. TRANSP simulations of the beam injection accurately reflect this measured anisotropy. In the high field configuration, the full neutral beam heating power of

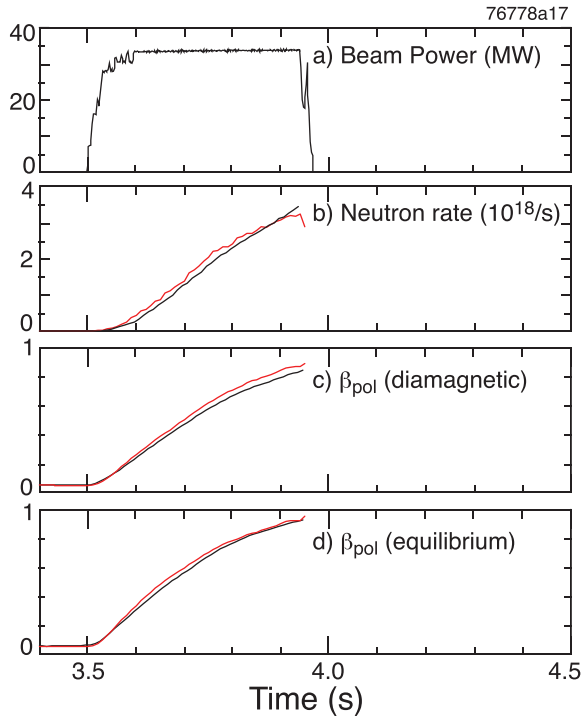

FIG. 3. Comparison of TRANSP simulations (red) with measured time evolution (black) of the (b) neutron rate, (c) diamagnetic β_{pol} (i.e., measured with a diamagnetic loop) and (d) equilibrium β_{pol} ($I_P = 2.5$ MA, $B_{tor} = 5.2$ T).

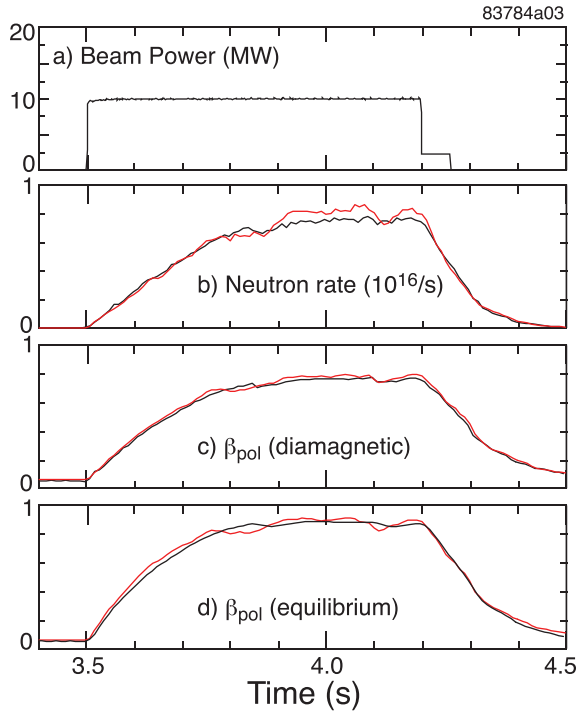

FIG. 4. Comparison of TRANSP simulations (red) with measured time evolution (black) of the (b) neutron rate, (c) diamagnetic β_{pol} (i.e., measured with a diamagnetic loop) and (d) equilibrium β_{pol}.

≈35 MW is just adequate to reach the empirical beta limit of $\beta_n \approx 2$.

Similar good agreement is found for the low field discharges where $\beta_n \leq 2$, as illustrated in Figs. 4(a)–4(d). This shot has deuterium beams injected into a predominantly

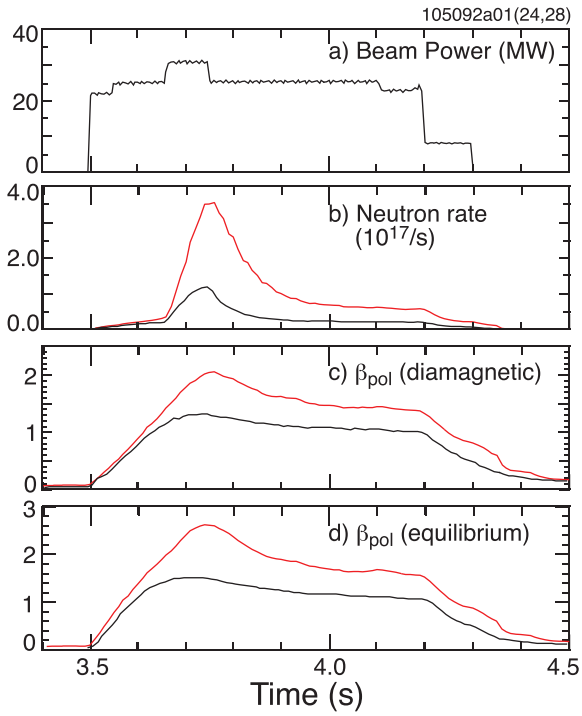

FIG. 5. Comparison of TRANSP simulations (red) with measured time evolution (black) of the (b) neutron rate, (c) diamagnetic β_{pol} (i.e., measured with a diamagnetic loop) and (d) equilibrium β_{pol}.

deuterium target plasma, rather than the mixed deuterium-tritium neutral beam injection of the high field comparison shot. There are still trace amounts of tritium in the plasma from wall recycling, which result in a significant D-T neutron rate. As the exact level of trace tritium is uncertain, this parameter is adjusted in TRANSP to match the measured neutron rate; comparison of experimental and TRANSP predictions of neutron rate are thus of less value in D-only shots taken after the start of the tritium campaign. This trace amount changes relatively slowly shot-to-shot and a constant recycling fraction of 1.9% tritium was used in this TRANSP run to match the neutron rate evolution.

In the low field cases, no clear disruptive beta limit was reached with the available beam power (≈30 MW) although $\beta_n > 3$ was transiently reached at the highest beam powers. In Fig. 5 is shown a low field example with ≈30 MW of neutral beam heating, including a 100 ms pulse of tritium beams from 3.65 s to 3.75 s. Although the β_n briefly exceeds 3, there is no disruption, but rather energy confinement limits the achievable β. For this case, the TRANSP simulations (red), including the neutron rate simulation, greatly overestimate the fast ion content of the plasma (thermal kinetic parameters are measured, as above). The time at which the TRANSP simulations begin to clearly diverge from the experimental measurements is uncertain, but the agreement worsens noticeably after 3.6 s.

In this shot, a short blip of Tritium neutral beams was injected from 3.65 s to 3.75 s during which the neutron rate is the sum of the T-beam on D-beam, T-beam on D-thermal and D-beam on T-thermal neutron rates. For the low field shots the thermal DT reaction rate is negligible. The neutron rate is then proportional to either the fast ion density to the first or second power and a good indication of the fast ion density and is largely insensitive to trace-tritium recycling from the wall. Despite this the neutron rate predicted by TRANSP during the tritium beam blip also greatly exceeds the measured neutron rate. A similar tritium beam-blip experiment done in reversed-shear TFTR plasmas also found a significant, unexplained discrepancy between the predicted and measured neutron rates.[17]

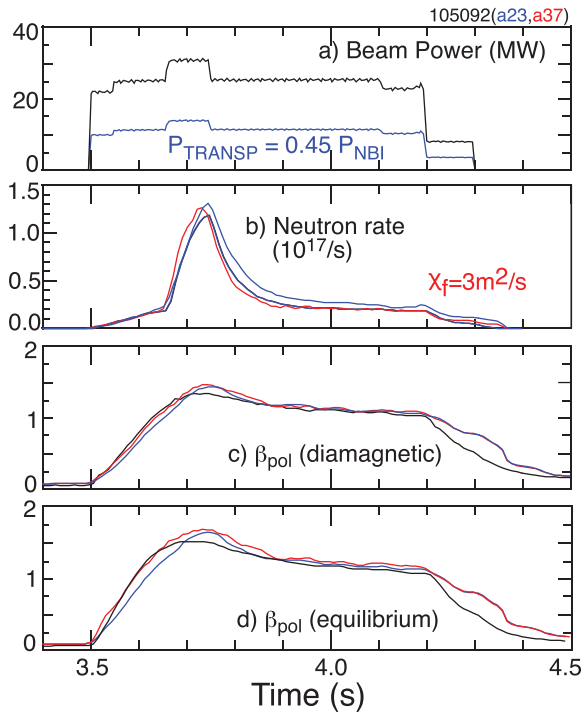

FIG. 6. Comparison of TRANSP simulations with 45% of the beam power (blue) and with enhanced fast ion diffusivity (red) with the measured time evolution (black) of the b) neutron rate, c) diamagnetic β_{pol} (*i.e.*, measured with a diamagnetic loop) and d) equilibrium β_{pol}.

To summarize, TRANSP simulations of high field shots for a range of heating powers and poloidal betas, $0.3 \leq \beta_{pol} \leq 2$ typically find reasonably good agreement (±10%) in the stored energy and neutron rates (Fig. 3 and see also Fig. 2). Similarly, at low field, TRANSP predicts neutron rates and stored energies reasonably well for $\beta_{pol} < 0.9$ (c.f., Figs. 2 and 4). However, at low field, it was possible to reach $\beta_{pol} \geq 1.5$ with higher beam power without encountering the fast disruptions seen at higher toroidal field. In this range, TRANSP predictions showed increasing disagreement with both neutron rate and stored energy as β_{pol} increased (c.f., Figs. 2 and 4). At the highest betas, several types of fast-ion driven instabilities were seen, such as fishbones,[18,19] High Frequency Fishbones,[20–23] Toroidal Alfvén Eigenmodes (TAE)[24,25] and a mode which was previously identified as an Axi-symmetric Beam-driven Mode (ABM),[26] but, in light of subsequent theoretical developments, has come to be known as the Geodesic Acoustic Mode (GAM).[27–29]

For the high power, high β_n shot shown in Fig. 5, both the stored energy and the neutron rate can be matched by artificially reducing the input beam power by ≈45%, including the source power for the tritium beam blip (blue curves, Fig. 6). For this postulated loss fraction, TRANSP underestimates the stored energy for the first 200 ms of neutral beam injection (Fig. 7). A similar good match to stored energy and neutron rate evolution can be made by introducing an enhanced fast ion diffusivity of ≈2.7 m^2/s to 3.65 s (also Fig. 7, red curves). There are other models that could be applied to model fast ion loss mechanisms, but the choice of model, in the absence of more data is somewhat arbitrary. This introduces uncertainty in the fast ion pressure profile and thus in the calculations of the ideal stability.

III. DISCUSSION OF ANOMALOUS PROCESSES

Enhanced losses of fast ions could arise for a number of reasons. Firstly, the higher beta will shift the magnetic axis outwards, which could in principle enhance classical ripple losses. However, the apparent onset of losses above a threshold in beta (or beam power) suggests an instability is responsible. The instability could be resonantly driven by the beam ions, as with TAE modes, or an ideal instability might onset above some beta threshold. Or the threshold could indicate a change in the character of an existing instability, for example, the electro-magnetic component of micro-instabilities increases with plasma beta and may enhance fast ion transport. In this section, the correlation of instability onsets with fast ion confinement degradation will be examined.

There are several types of MHD modes seen in at least some instances which might enhance fast ion losses early in

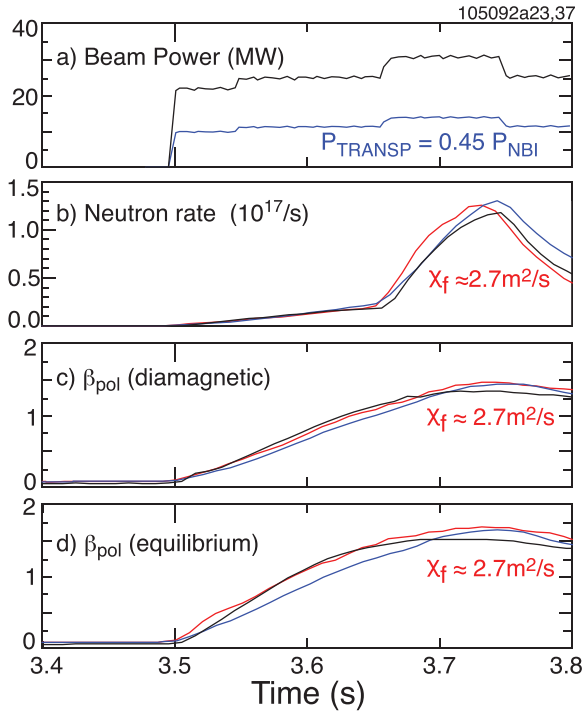

FIG. 7. Expanded timescale for Fig. 6 showing TRANSP simulations with 45% of beam power (blue) and with an enhanced fast ion diffusivity of ≈2.7 m^2/s (red).

the beam injection phase. In Fig. 8 is shown a spectrogram from a high power, low field discharge which exhibits most of the instability activity seen in these plasmas. There are four types of bursting, coherent mode activity. The Axi-symmetric Beam-driven Modes (ABM) are indicated in red in the frequency range from 10 kHz to 30 kHz. The high frequency branch of fishbones are seen in blue in the frequency range from 40 kHz to 80 kHz, starting at 3.54 s. Conventional fishbones and the normal, low frequency fishbones are seen below 20 kHz after 3.59 s. The Toroidal Alfvén Eigenmodes onset at 3.6 s at frequencies between

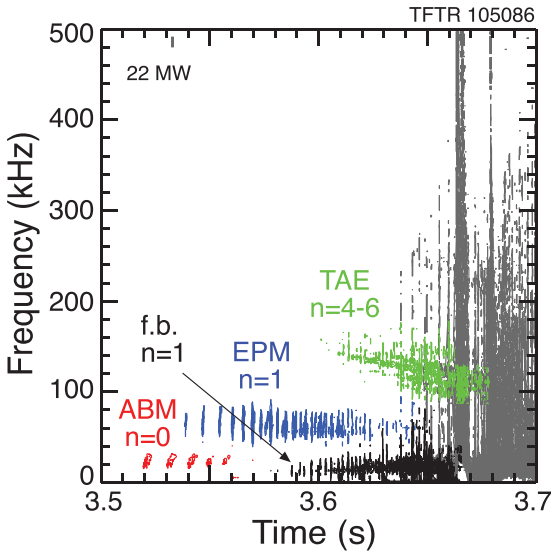

FIG. 8. Spectrogram of magnetic fluctuations showing a variety of energetic particle driven instabilities in the first 200 ms of NBI heating.

100 kHz and 150 kHz (green). A quasi-coherent mode commonly seen in TFTR plasmas, the Alfvén Range of Frequency mode (ARF), or sometimes the Alfvén Frequency Mode (AFM)[30] is barely visible in this shot in the frequency range of 200 kHz to 240 kHz but is commonly seen in shots without apparent fast ion losses and is therefore not considered a candidate for driving fast ion losses. More instabilities will occur later in the beam heating phase, but the anomalous fast ion losses appear to begin very early in the beam injection phase. In Secs. III A–III C, we will investigate the correlation of ABMs, EPMs and fishbones with the inferred anomalous fast ion losses.

A. Geodesic acoustic modes (GAMs)

The first modes to appear after the start of NBI injection are low frequency, chirping bursting modes with toroidal mode number of zero and a standing-wave structure in the poloidal direction (e.g., Fig. 8, red contours). The frequency in this case chirps upwards, but downward frequency chirps, or occasionally in both directions is also seen. The first observations of these modes were reported in 1989 (Ref. 26) where they were referred to as Axi-symmetric Beam-driven Modes (ABMs). The ABMs are often seen during the first 50 ms to 100 ms of neutral beam injection at both low and high field. They are more commonly seen with counter-tangential beam injection but were also seen in some cases with only co-tangential beam injection. The modes are not large in amplitude, typically appear only briefly in the initial phase of beam heating, and their appearance has not been correlated with significant fast ion losses on TFTR. Thus, initially, interest in these modes on TFTR was low. However, the observation that what appears to be a similar mode on DIII-D is, however, correlated with strong fast ion losses, suggests that these modes might be responsible for some or all of the anomalous fast ion losses seen here.

The fundamental characteristics of the ABM/GAM were reported previously, and Fig. 9 is adapted from the earlier work.[26] The ABM has a standing wave nature of the mode, which has nodes in the magnetic fluctuations on the mid-plane, and, for the $m = 2$ mode, at roughly 90° above and below, with the amplitude peaked between the nodes. The modes are identified by their typically standing wave (or partially standing wave) structure and often have a toroidal wavenumber, $n = 0$ (i.e., axisymmetric), similar to the expected structure of GAMs. However, examples of similar modes with toroidal mode numbers of $n = 1$ and $n = 2$ were also seen. The mode frequency was noted to be comparable to the sound wave frequency ($=mC_S/qR$), and resonant with the beam ion poloidal transit frequency.[26] The modes are well below the shear-Alfvén frequencies ($=mV_{Alfvén}/qR$) and well above the drift frequencies. These observations predated the theoretical work on what were identified as the energetic-particle-driven Geodesic Acoustic Modes (GAMs) on JET[27] and DIII-D.[28,29] These mode characteristics, frequency, toroidal and poloidal structure, are consistent with the theoretical predictions for eGAMs as described for DIII-D plasmas.[28]

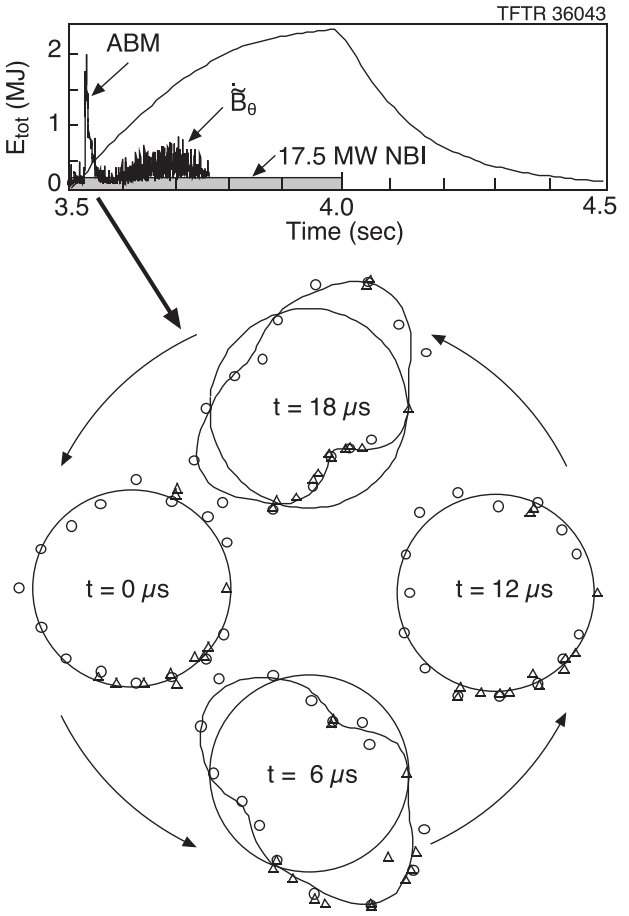

FIG. 9. (a) Traces showing the rise in stored energy and the amplitude of the rms $\partial B/\partial t$ signal, (b) Poloidal plot of mode amplitude for all coils, with toroidally separated coils mapped to same toroidal plane assuming $n = 0$.

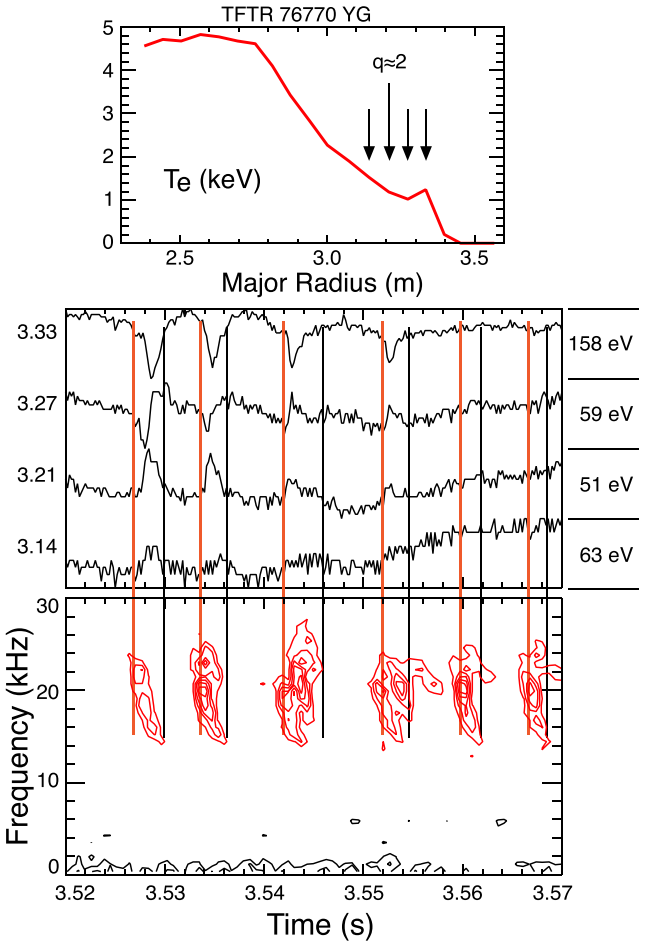

FIG. 10. (a) Electron temperature profile measured with GPC, arrows show locations of channels plotted in, (b) four GPC channels showing effect of GAM bursts on edge electron temperature, (c) spectrogram showing frequency evolution of GAM bursts.

While no clear evidence was found on TFTR that the ABM/GAM caused fast ion losses, in some instances the ABM/GAM did affect the electron thermal transport, causing perturbations in the edge temperature, which might be interpreted as the formation of a transient transport barrier. In Fig. 10 are shown GAMs from a high field shot very similar to the one shown in Figs. 1 and 3. This shot had slightly lower β and did not disrupt. Very early in the neutral beam heating phase (20 ms to 70 ms after start of NBI), downward chirping GAMS were seen (shown in Fig. 10(c)). Coincident with each of the first four GAM bursts, there is a small (3–4%) increase in electron temperature inside a major radius of about 3.27 m (the outboard plasma edge is at 3.4 m) as measured with the Grating Polychromator (GPC) used for fast ($\approx$200 kHz) measurements of the electron cyclotron emission (ECE).[13] The temperature perturbation is localized to the outer 30 cm of the plasma. Note that the EC emission for the outermost channel shown in Fig. 10(b) ($R = 3.33$ m) is becoming non-thermal and the emission does not represent a local electron temperature.

The ABM/GAMs seen in the low field, high-β shots have very similar mode characteristics. A spectrogram showing the ABM in a 2 T shot is shown in Fig. 11. The ABM/GAM are shown in red; the blue contours show high-frequency fishbones. The magnetic fluctuations as measured with a Mirnov coil are shown in Fig. 11(b) and expanded over a 1 ms interval in Fig. 11(c). Expanded in time, it is seen that the ABM fluctuations have a beating character, suggesting the presence of two modes of similar amplitude whose frequencies are separated by about 5 kHz.

In Fig. 12, the phase and amplitude vs. poloidal angle of the magnetic fluctuations is shown. The relative phase shows a nearly step-like behavior on the outboard side (between 90° and 270° in Fig. 12) and the amplitude shows anti-nodes above and below the midplane, as expected for a standing wave. However, on the inboard side, the modes are much weaker and the phase indicates more of a traveling-wave character. The solid lines in the figure are the phase and amplitude for a mixed traveling wave plus a standing wave with a ballooning character, with parameters chosen to fit the data. The mode shows up as multiple bursts, with each burst having a relatively weak upward frequency chirp, from $\approx$18 kHz to $\approx$32 kHz. The relative magnetic fluctuation level was larger than for the high field shots, $^{TM}B/B \approx 10^{-6}$ vs $^{TM}B/B \approx 2 \times 10^{-7}$.

Internal measurements were more difficult at these low fields for TFTR diagnostics, and no evidence of the modes was seen on either of the fast ECE diagnostics (which, in any event, were not configured to view the plasma edge), or on

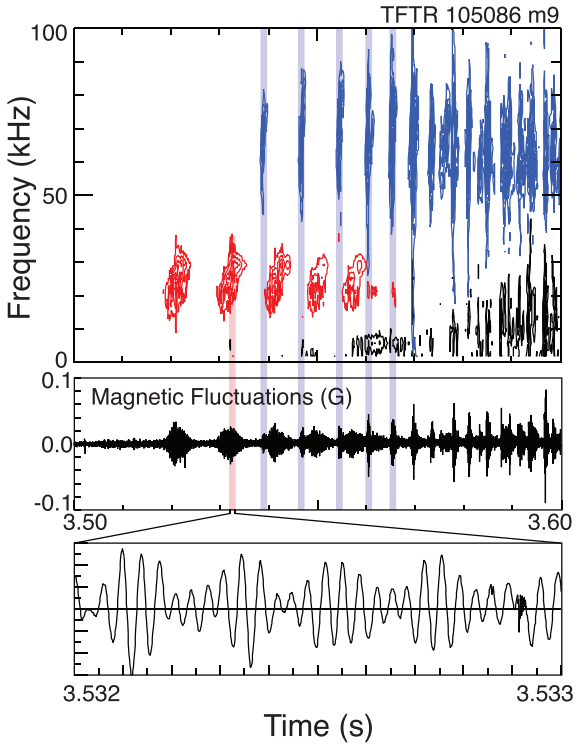

FIG. 11. (a) Spectrogram of magnetic fluctuation signal showing GAM bursts (red) and EPM bursts (blue), (b) magnetic fluctuations, (c) expanded time base showing beating of multiple modes during GAM burst.

the soft x-ray cameras (although these were not well matched to the relatively low temperatures and densities of these plasmas). The modes are present early in the beam heating phase, before the beta reaches the threshold, suggested in Fig. 2, where anomalous fast ion losses are expected. Thus, the mode existence is correlated more with the neutral beam power or fast ion population, rather than β. This could be consistent with the TRANSP simulations, which were ambiguous as to the time of onset of the fast-ion confinement discrepancy. The ABMs are not detected following about 3.56 s, but if they are indeed GAM, they would be predominantly electrostatic and possibly are not detected with the Mirnov system.

The beam ion deposition at the time of the appearance of these modes has not developed the equilibrium slowing-down distribution, but still retains a strong bump-on-tail character (Fig. 13(a)). Resonance conditions are explored for the full and half energy beam ions. The pitch-angle distribution of the half-energy beam ions is shown in Fig. 13(b) for a range of radii from r/a = 0.15 to r/a = 0.75. The beam ions are mostly co-passing with pitch angles greater than about 0.7. However, the pitch angle distribution extends to pitches of ≈0.5 around the mid-radius. The poloidal transit frequency for co-tangential and counter tangential injected ions [with pitch = ±0.5 and at full (100 keV and ≈half (45 keV) energy], vs. the birth radius are shown in Fig. 14. Both co and counter beam ions near the passing-trapped boundary, and trapped beam ions have poloidal transit frequencies near the mode frequency. As the modes are axi-symmetric, the toroidal transit frequency is irrelevant. Thus, a plausible drive resonance for these modes is through the beam poloidal transit frequency (or bounce frequency for trapped ions).[26,27]

The observed ABM/GAM frequency is compared to f_{TAE} (the frequency of the center of the TAE gap), f_{GAM} [$= C_S/(2\pi R)$] and the drift wave frequency in Fig. 14. Here, f_{GAM} [$= C_S/(2\pi R)$] is used for the GAM frequency, where $C_s = 9.79 \times 103$ * $((T_e(\text{eV}) + 1.75\ T_i(\text{eV}))/2)^{1/2}$ m/s; smaller by ≈1.4 than that predicted.[27] The mode frequency range is indicated by the shaded region and is more consistent with acoustic branch modes[26,28] than Alfvén frequency.

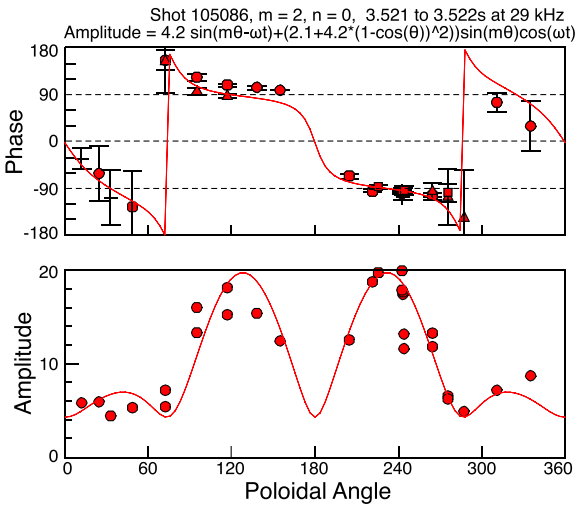

FIG. 12. Experimental phase and amplitude data fit with combination standing and traveling wave analytic functions Amplitude = 4.2 $\sin(m\theta-\omega t) + (2.1 + 4.2*(1-\cos(\theta))^2))\sin(m\theta)\cos(\omega t)$; a) relative phase of magnetic fluctuations vs. poloidal angle, b) mode amplitude.

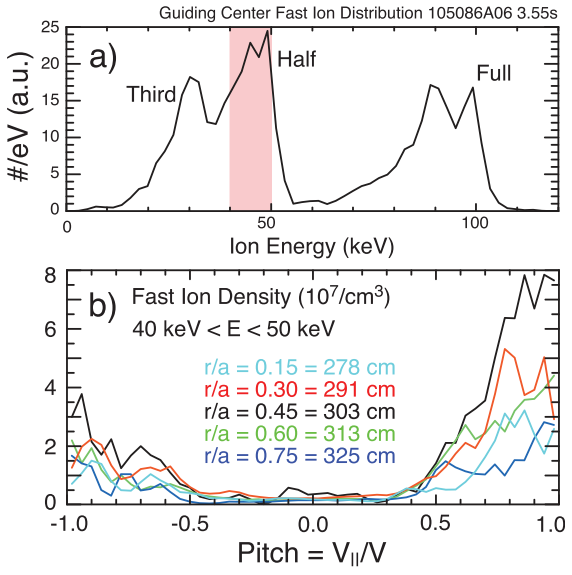

FIG. 13. (a) Energy distribution for beam ions 50 ms after start of beam injection, (b) pitch distribution for intermediate energy fast ions at different radii.

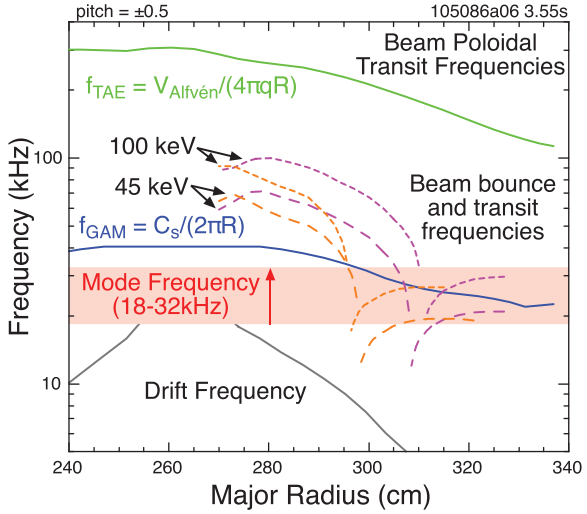

FIG. 14. Profiles of TAE gap center frequency, GAM frequency and drift frequency. Beam bounce and poloidal transit frequencies (100 keV/45 keV - short/long dashes, pitch = 0.5 (co) - magenta, pitch = −0.5 (ctr) - orange). Shaded region shows range of frequency chirps.

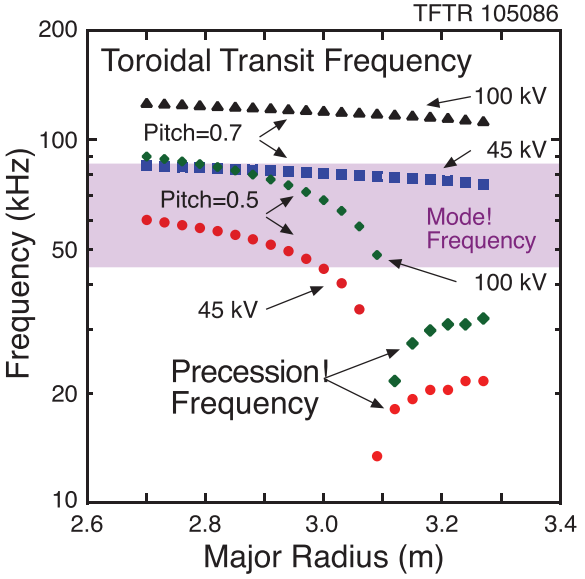

FIG. 16. Toroidal transit frequency for co-passing beam ions at 45 keV and 100 keV and pitches of 0.5 and 0.7. Shaded area is mode frequency chirp range.

B. Fishbone/EPM

There are two branches of the fishbone mode. The more common fishbone is excited through a resonance with the precession frequency of fast ions from neutral beam injection. The mode is the n = 1 internal kink, and onsets at the upper range of beam ion precession frequencies where the energy transfer from ions to modes is fastest. As the ions are expelled, the frequency sweeps down towards zero in the plasma frame, sweeping fast ions out along the way.[18] These "classical" fishbones are seen after about 3.6 s between 10 and 20 kHz. The bursts are very short, and a frequency chirp, if present, is difficult to measure.

A second higher frequency fishbone-like mode appears in these shots after ≈3.55 s in the frequency range from about 50 kHz up to 85 kHz (blue contours in Fig. 11 and an expanded view in Fig. 15. These are identified as high frequency fishbones (HHFB), first identified on JET, where they are believed to be excited through a precession-drift resonance with the much more energetic ions expected for minority RF heating experiments.[20,21] The modes appear in a sequence of bursts, with each burst lasting ≈1 ms during which the mode frequency chirps upward from ≈50 kHz up to ≈85 kHz. The toroidal mode number is n = 1 and the modes propagate in the co-parallel direction. Neutron rate measurements at a 1 kHz sampling rate did not show measurable, correlated drops greater than the noise level of 2–3%.

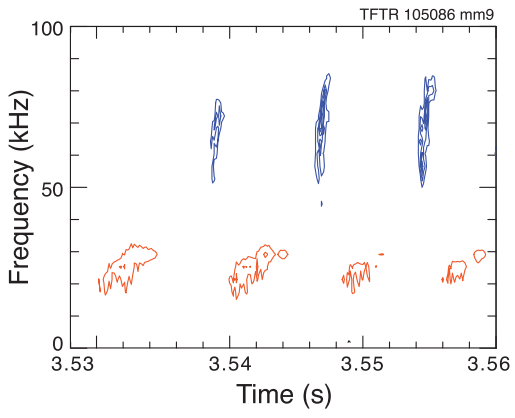

FIG. 15. Spectrogram of Mirnov coil showing High Frequency Fishbones (blue) and GAM (red).

The frequency of these modes is much higher than the beam-ion precession frequency, which is below 10 kHz. The bounce frequency for trapped fast ions is below 25 kHz for these parameters and the precession frequencies of trapped beam ions are also below the mode onset frequency. In this case, it appears that the modes are excited through a resonance similar to that which excites the TAE, that is through a resonance with the toroidal transit frequency of beam ions with pitch between 0.5 and 0.7 (Fig. 16). The upward frequency chirp suggests that the optimum energy transfer between beam ions and energetic particles occurs around 50 kHz. This is close to the nominal GAM/BAE frequency and that may also explain the initial mode frequency. Most beam ions have pitch larger than 0.5, whereas there are not many fast ions which can maintain the toroidal transit resonance at frequencies below about 45 kHz, which may explain the upward frequency chirping.

The HFFB onset may be early enough to explain the inferred β_{fast} discrepancy. There are no internal measurements of the mode amplitude, but Fig. 17 shows the scaling of the amplitude, as measured with Mirnov coils, against the discrepancy between TRANSP modeling and the experimental ®. The HFFB appear at ®'s where fast ion losses are inferred to begin and become larger as ® is increased, although this correlation may be coincidental. It would also be expected that as the fast ion beta was increased, the drive for the HFFBs would become larger and mode amplitudes would increase. And as pointed out above, there are no direct experimental data correlating the HFFB bursts with fast ion losses.

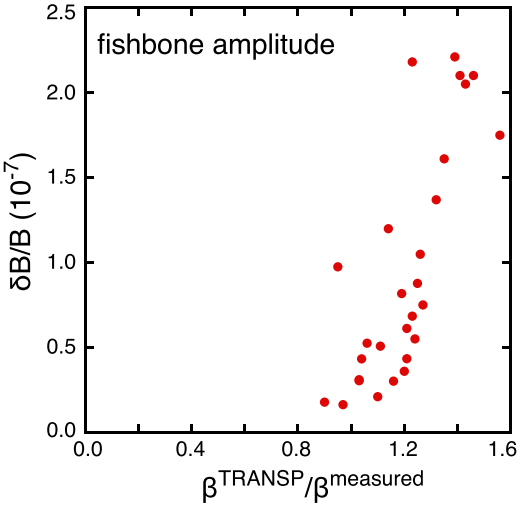

FIG. 17. Amplitude of fishbones vs. discrepancy in TRANSP predicted beta vs. measured beta.

C. Toroidal Alfvén eigenmodes

In Fig. 8, it was seen that the TAE onset around 3.6 s, as the high frequency fishbones were dying out. The same data are shown in Fig. 18 with higher time resolutions, and the rms magnetic fluctuation level is also shown, illustrating the bursting character of the TAE at onset. At this toroidal field and density, the full-energy beam ion velocity is less than the core Alfvén speed, so these modes are likely excited by the "1/3" resonance with the beam ions.[24] Beam-driven Toroidal Alfvén Eigenmodes have been extensively studied on TFTR in low field plasmas with toroidal fields from 1 T up to 3.5 T. The TAE experiments were typically done in plasmas with a lower plasma current than for the experiments described here, that is, $I_P = 0.4$ MA rather than 1.0 MA. In these experiments, the TAE showed a strong bursting character, although without the frequency chirps that are commonly seen for TAE on NSTX or MAST. Note that the TAE bursts are strongly correlated with the HFFB and fishbone bursts. In these previous experiments, a roughly linear scaling of fast ion losses, deduced from neutron rate drops,

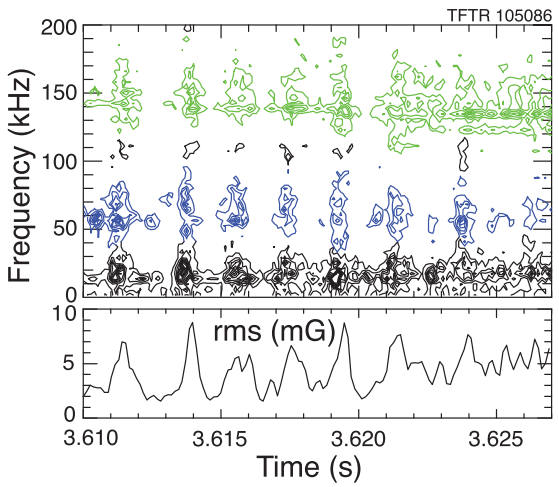

FIG. 18. (a) Spectrogram showing TAE (green), HHFB (blue), and fishbones (black), (b) rms amplitude of TAE magnetic fluctuation.

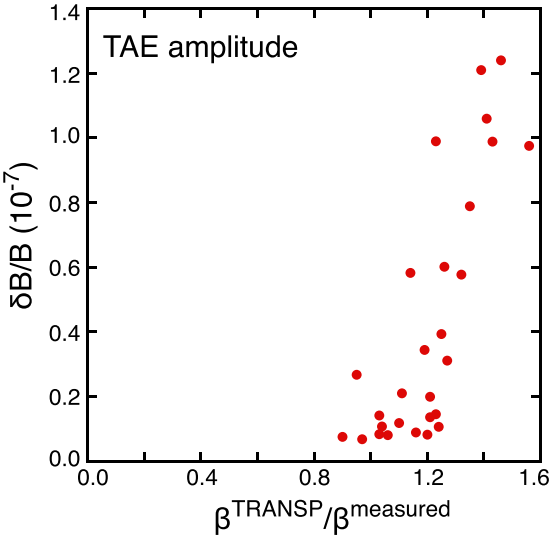

FIG. 19. Amplitude of TAE vs. discrepancy in TRANSP predicted beta vs. measured beta.

with TAE amplitude was found.[31] The absolute burst amplitudes here are comparable to those seen in the lower current, lower field experiments where neutron drops of up to 10% were seen.

As seen in Fig. 19, the amplitude of the TAE scales with the discrepancy between the TRANSP prediction of β and the measured value. However, the amplitudes are small and the onset occurs later than needed to explain the inferred fast ion loss anomaly evolution. The correlation of TAE amplitude may reflect a combination of higher fast ion beta, higher density in the high beam power shots, which improves the marginal resonance by lowering the TAE frequency and increasing the drive.

IV. DISCUSSION OF FAST ION LOSSES

The effect of periodic losses on the "saturated" neutron rate can be estimated assuming that the early evolution of the neutron rate approximately follows an exponential approach to saturation. The period of the TAE, HHFB, and FB bursts is $\tau_{period} \approx 2$ ms. The classical fast-ion slowing down time is 65–80 ms in the core region, and the early neutron rate evolution for a similar shot, without the tritium NBI, has an exponential timescale of $\tau_{slow} \approx 100$ ms, roughly consistent with this slowing-down time estimate. The TRANSP neutron rate prediction has large uncertainties due to the presence of trace amounts of tritium, but the measured neutron rate appears to be of order 50% to 60% of the TRANSP prediction, with about 80% of the neutron production from beam ion on thermal deuterium and tritium reactions, which is insensitive to the tritium recycling. We assume that the neutron rate without MHD is approximately of the form $S/S_0 \approx (1 - \exp(-t/\tau_{slow}))$, where S_0 would be the saturated neutron rate in absence of losses. With these parameters and this form of time dependence, periodic losses of order 2% every 2 ms could account for the neutron rate discrepancy, and beta deficit. As neutron rate drops of order 10% were seen for TAE bursts of comparable magnitude, albeit in lower current, lower field plasmas, the assumption

of 2% fast-ion losses at each TAE/HFFB/FB burst would seem not unreasonable. Of course, plasma density and electron temperature are both evolving during this period, so this estimate illustrates only that the observations might be consistent with this model.

V. SUMMARY

Experiments to investigate the dependence of β-limiting disruption characteristics on toroidal field strength in TFTR failed to produce hard disruptions at low field, even for β's 50% higher than the empirical β-limit of $\beta_n \approx 2$ at high field. We postulate that this difference in behavior may result from the development of anomalous, i.e., non-classical, losses of energetic ions from the neutral beam heating. Comparisons of experimentally measured β's to TRANSP simulations suggest anomalous loss of up to half of the beam fast ions in the highest β, low field shots. Toroidal Alfvén eigenmodes, and both a new High Frequency fishbone, and classical fishbone instabilities are seen early in the beam heating phase. The amplitude of the High Frequency Fishbones and TAE increases above the threshold beta for inferred fast ion losses. Although no direct evidence exists for these inferred enhanced fast ion losses, losses of a few percent for each fishbone/TAE burst could explain the inferred deficit in fast ions. The anomalous fast ion transport may at the same time broaden the pressure profile, increasing the beta-limit. We have presented the first observations of high frequency fishbones[20–23] on TFTR. We find that, unlike the JET observations, these modes are likely excited through a toroidal transit frequency resonance with the beam ions.

Axi-symmetric Beam-driven Modes (ABMs) are also seen early in the beam heating phase. Comparison of the characteristics of the ABMs[26] suggests that they are the same as the Geodesic Acoustic Modes seen on JET[27] and DIII-D.[28] The ABM spatial structure ($n = 0$ and a standing wave in the poloidal direction) and resonance with the poloidal transit frequency are the same as reported for the GAM. On DIII-D the GAM were correlated with fast ion losses, however, on TFTR that does not seem to be the case. However, under some conditions, there does appear to be a transient transport barrier formed near the $q = 2$ surface with each ABM/GAM burst.

ACKNOWLEDGMENTS

We would like to express our appreciation to the TFTR team, with special thanks for T. Carroll, L. Nixon, R. Reed, and C. Scimeca for support in recovering TFTR data. This work was supported under U.S. DoE Contract Nos. DE-AC02-76CH03073 and DE-AC02-09CH11466.

[1]D. Meade and the TFTR Group, in *Proceedings of the International Conference on Plasma Physics and Controlled Nuclear Fusion, Washington, DC, 1990* (International Atomic Energy Agency, Vienna, 1991), Vol. I, pp. 9–14.
[2]E. D. Fredrickson, K. McGuire, Z. Chang, A. Janos, M. Bell, R. V. Budny, C. E. Bush, J. Manickam, H. Mynick, R. Nazikian, and G. Taylor, "β limit disruptions in the tokamak fusion test reactor," Phys. Plasmas **2**, 4216 (1995).
[3]W. Park, E. D. Fredrickson, A. Janos, J. Manickam, and W. M. Tang, Phys. Rev. Lett. **75**, 1763 (1995).
[4]E. D. Fredrickson, K. M. McGuire, Z. Y. Chang, A. Janos, J. Manickam, G. Taylor, S. Mirnov, I. Semenov, D. Kislov, and D. Martynov, "Ballooning instability precursors to high β disruptions," Phys. Plasmas **3**, 2620 (1996).
[5]E. D. Fredrickson, S. A. Sabbagh, M. G. Bell, D. Mansfield, S. Batha, Z. Chang, F. Levinton, K. M. McGuire, M. Okabayashi, G. Taylor, H. Takahashi, M. Hughes, J. Manickam, M. Phillips, and L. Zakharov, "The stability of advanced operational regimes on TFTR," Phys. Plasmas **4**, 1589 (1997).
[6]R. Kaita, R. B. White, A. W. Morris, E. D. Fredrickson, K. M. McGuire, S. S. Medley, T. J. Murphy, and S. D. Scott, Phys. Fluids B **2**, 1584 (1990).
[7]Z. Chang, E. D. Fredrickson, J. D. Callen, K. M. McGuire, M. G. Bel, R. B. Budny, C. E. Bush, D. S. Darrow, A. C. Janos, L. C. Johnson, H. K. Park, S. D. Scott, J. D. Strachan, E. J. Synakowski, G. Taylor, R. M. Wieland, M. C. Zarnstorff, S. J. Zweben, and the TFTR Team, "Transport effects of low (m,n) MHD modes on TFTR supershots," Nucl. Fusion **34**, 1309 (1994).
[8]Z. Chang, E. D. Fredrickson, S. H. Batha, M. G. Bell, R. V. Budny, F. M. Levinton, K. M. McGuire, G. Taylor, M. C. Zarnstorff, and the TFTR Group, "Neoclassical tearing modes in tokamak fusion test reactor experiments. I. Measurements of magnetic islands and Δ'," Phys. Plasmas **5**, 1076 (1998).
[9]R. V. Budny, Nucl. Fusion **34**, 1247 (1994).
[10]A. Pankin, D. McCune, R. Andre, G. Bateman, and A. Kritz, Comput. Phys. Commun. **159**, 157–184 (2004).
[11]F. M. Levinton, L. Zakharov, S. H. Batha, J. Manickam, and M. C. Zarnstorff, Phys. Rev. Lett. **72**, 2895 (1994).
[12]F. Troyon, H. Gruber, H. Saurenmann, S. Semenzato, and S. Succi, Plasma Phys. Controlled Fusion **26**, 209 (1984).
[13]A. Cavallo, R. C. Cutler, and M. P. McCarthy, Rev. Sci. Instrum. **59**, 889 (1988).
[14]G. Taylor, P. C. Efthimion, M. P. McCarthy, E. Fredd, and R. C. Cutler, Rev. Sci. Instrum. **57**, 1974 (1986).
[15]C. E. Bush, R. E. Bell, and E. J. Synakowski, Rev. Sci. Instrum. **66**, 642 (1995).
[16]H. Park, D. K. Mansfield, L. C. Johnson, and C. H. Ma, Rev. Sci. Instrum. **56**, 938 (1985).
[17]E. Ruskov, R. V. Budny, D. C. McCune, S. S. Medley, M. H. Redi, S. Scott, E. J. Synakowski, S. von Goeler, R. B. White, and S. J. Zweben, "Beam ion loss in TFTR reversed magnetic shear plasmas," Phys. Rev. Lett. **82**, 924 (1999).
[18]R. B. White, R. J. Goldston, K. M. McGuire, A. H. Boozer, D. A. Monticello, and W. Park, Phys. Fluids **26**, 2958 (1983).
[19]L. Chen, R. B. White, and M. N. Rosenbluth, Phys. Rev. Lett. **52**, 1122 (1984).
[20]F. Nabais, D. Borba, M. Mantsinen, M. F. F. Nave, and S. E. Sharapov, Phys. Plasmas **12**, 102509 (2005).
[21]F. Zonca, L. Chen, A. Botrugno, P. Buratti, A. Cardinali, R. Cesario, V. Pericoli Ridolfini, and JET-EFDA contributors, "High-frequency fishbones at jet: Theoretical interpretation of experimental observations," Nucl. Fusion **49**, 085009 (2009).
[22]Z. Fulvio and C. Liu, Phys. Plasmas **21**, 072120 (2014).
[23]Z. Fulvio and C. Liu, Phys. Plasmas **21**, 072121 (2014).
[24]W. W. Heidbrink, Phys. Plasmas **15**, 055501 (2008).
[25]K. L. Wong, Plasma Phys. Controlled. Fusion **41**, R1 (1999).
[26]*Axi-Symmetric Beam-Driven Modes During High Power NBI on TFTR*, edited by E. D. Fredrickson, K. McGuire, R. J. Goldston, and C. Z. Cheng, in *Sixteenth European Conference on Controlled Fusion and Plasma Physics, Venice, Italy, March 1989* (in Proceedings of the Thirteenth European Conference on Controlled Fusion and Plasma Physics) (Venice, Italy, March 1989) Europhysics Conference Abstracts, Vol. (13b), Part II, pp. 477-480.
[27]H. L. Berk, C. J. Boswell, D. Borba, A. C. A. Figueiredo, T. Johnson, M. F. F. Nave, S. D. Pinches, and S. E. Sharapov, Nucl. Fusion **46**, S888 (2006).
[28]G. Y. Fu, "Energetic-particle-induced geodesic acoustic mode," Phys. Rev. Lett. **101**, 185002 (2008).
[29]R. Nazikian, G. Y. Fu, M. E. Austin, H. L. Berk, R. V. Budny, N. N. Gorelenkov, W. W. Heidbrink, C. T. Holcomb, G. J. Kramer, G. R. McKee, M. A. Makowski, W. M. Solomon, M. Shafer, E. J. Strait, and M. A. Van Zeeland, "Intense geodesic acoustic-like modes driven by suprathermal ions in a tokamak plasma," Phys. Plasmas **15**, 056107 (2008).

[30]Z. Chang, E. D. Fredrickson, S. J. Zweben, H. K. Park, R. Nazikian, E. Mazzacuto, S. H. Batha, M. G. Bell, R. V. Budny, C. E. Bush, D. S. Darrow, D. Ernst', G. Y. Fu, R. J. Hawryluk, K. W. Hill, J. C. Hosea, A. C. Janos, D. L. Jassby, D. W. Johnson, L. C. Johnson, F. M. Levinton, D. K. Mansfield, K. M. McGuire, D. R. Mikkelsen, D. Mueller, D. K. Owens, A. T. Ramsey, S. A. Sabbagh, E. J. Synakowski, H. Takahashi, G. Taylor, M. E. Thompson, R. M. Wieland, K.-L. Wong, and M. C. Zarnstorff, "Alfvén frequency modes at the edge of TFTR plasmas," Nucl. Fusion **35**, 1469 (1995).

[31]D. S. Darrow, S. J. Zweben, Z. Chang, C. Z. Cheng, M. D. Diesso, E. D. Fredrickson, E. Mazzucato, R. Nazikian, C. K. Phillips, S. Popovichev, M. H. Redi, R. B. White, J. R. Wilson, and K.-l. Wong, "Losses due to Alfven Modes in TFTR," Nucl. Fusion **37**, 939 (1997).